Weakening Influence of Spring Soil Moisture over the Indo-China Peninsula on the Following Summer Mei-Yu Front and Precipitation Extremes over the Yangtze River Basin

CHUJIE GAO,[a,b] GEN LI,[a,c] AND BEI XU[b,d]

[a] College of Oceanography/Key Laboratory of Marine Hazards Forecasting, Ministry of Natural Resources/Key Laboratory of Ministry of Education for Coastal Disaster and Protection, Hohai University, Nanjing, China; [b] Key Laboratory of Meteorological Disaster, Ministry of Education, and Collaborative Innovation Center on Forecast and Evaluation of Meteorological Disasters, Nanjing University of Information Science and Technology, Nanjing, China; [c] Southern Marine Science and Engineering Guangdong Laboratory (Zhuhai), China; [d] College of Intelligent Science and Control Engineering, Jingling Institute of Technology, Nanjing, China

(Manuscript received 20 February 2020, in final form 15 July 2020)

ABSTRACT: The seasonal prediction of precipitation extremes over the Yangtze River basin (YRB) has always been a great challenge. This study investigated the effects of spring soil moisture over the Indo-China Peninsula (ICP) on the following summer mei-yu front and YRB precipitation extremes during 1961–2010. The results indicated that the frequency of summer YRB precipitation extremes was closely associated with the mei-yu front intensity, which exhibited a strong negative correlation with the preceding spring ICP soil moisture. However, the lingering climate influence of the ICP soil moisture was unstable, with an obvious weakening since the early 1990s. Due to its strong memory, an abnormally lower spring soil moisture over the ICP would increase local temperature until the summer by inducing less evapotranspiration. Before the early 1990s, the geopotential height elevation associated with the ICP heating affected the western Pacific subtropical high (WPSH), strengthening the southwesterly summer monsoon. Consequently, the mei-yu front was intensified as more warm, wet air was transported to the YRB, and local precipitation extremes also occurred more frequently associated with abnormal ascending motion mainly maintained by the warm temperature advection. In the early 1990s, the Asian summer monsoon underwent an abrupt shift, with the changing climatological states of the large-scale circulations. Therefore, the similar ICP heating induced by the anomalous soil moisture had different effects on the monsoonal circulation, resulting in weakened responses of the mei-yu front and YRB precipitation extremes since the early 1990s.

KEYWORDS: Atmosphere-land interaction; Atmospheric circulation; Extreme events; Monsoons; Evapotranspiration; Decadal variability

1. Introduction

The summer climate over the Yangtze River basin (YRB) is strongly influenced by the East Asian monsoon. The mei-yu, which is part of the East Asian summer monsoon system, is a major rainfall event over the YRB, and provides most of the local summer precipitation (Wang and LinHo 2002; He et al. 2007). During the mei-yu period, a quasi-steady rainband is located over the YRB (Sampe and Xie 2010), and local flood disasters induced by intense precipitation occur frequently, causing great losses to human life and the economy (Lu 2004; Zhai et al. 2005; Cen et al. 2015). For example, a summer flood induced by extreme local precipitation during the second mei-yu period of 1998 resulted in more than 3000 deaths and direct economic losses of more than 30 billion U.S. dollars (Huang et al. 1998; Zhou et al. 2005). It is therefore essential to explore the nature and causes of the interannual variability of summer precipitation extremes over the YRB.

In summer, the southwesterly monsoonal wind conveys moist and warm air from the Bay of Bengal and the Indo-China Peninsula (ICP) to southern China, where it meets the dry and cold air over the YRB. This forms a quasi-steady mei-yu rainband over the YRB, which is accompanied by a typical frontal structure (i.e., the mei-yu front) in the lower troposphere (Chen and Zhai 2015). Thus, the mei-yu is a unique phenomenon of the East Asian summer monsoon system, and demonstrates multiscale features from daily to weekly and from mesoscale to large scale (Ninomiya and Shibagaki 2007; Ding et al. 2007). Previous studies (Li and Lu 2017; Gao et al. 2019) have suggested that the mean state of the mei-yu front is strongly associated with variations of the monsoon system. Furthermore, it has obvious effects on summer precipitation in the YRB. The results of our recent study (Gao et al. 2019) indicated that the occurrence of summer precipitation extremes over the YRB might be closely related to the mean intensity of the mei-yu front, which is aligned with variations of the East Asian summer monsoon.

The East Asian summer monsoon is a complex system, and is affected by various factors (e.g., Wang et al. 2000; Wu et al. 2009; Wang and Chen 2012). Essentially, the monsoon is induced by the sea–land temperature contrast, and thus the land surface thermal conditions are crucial to the monsoon system (Wu and Qian 2003; Wu et al. 2007; Zhang et al. 2017). Soil moisture, as one of the most important driving factors of local thermal conditions, has a large impact on the East Asian summer monsoon (Webster 1983; Zhang and Zuo 2011). In monsoonal regions, soil moisture can modulate the local thermal conditions, and thus the state of the atmosphere,

Corresponding author: Gen Li, ligen@hhu.edu.cn

DOI: 10.1175/JCLI-D-20-0117.1

eventually having a significant remote control of the monsoonal precipitation (Douville et al. 2001; Douville 2002). In East Asia, previous studies have revealed that the large-scale summer monsoonal circulation can be affected by anomalous surface heating associated with abnormal soil moisture in the premonsoon season (Zhang and Zuo 2011). For example, the spring soil moisture anomaly over the YRB to northern China has been shown to have a key role in modulating the land–sea thermal contrast, thus affecting the East Asian monsoonal circulation and precipitation in the following summer (Zuo and Zhang 2016; Liu et al. 2017).

Located in the upper reaches of the summer southwesterly monsoonal wind flow, the ICP land surface thermal conditions are crucial to the East Asian summer monsoon (Chen and Chen 1991; Zhang and Qian 2002; Jin et al. 2006). It was recently reported that an abnormal sensible heating exists in association with the ICP soil moisture anomaly in spring, and has a distinct influence on the onset and development of the East Asian summer monsoon (Ma et al. 2018). Gao et al. (2019) also found that the ICP soil moisture anomaly in the preceding spring could lead to an abnormal mei-yu front by affecting the East Asian monsoonal circulation, ultimately influencing the summer climate states (including precipitation and temperature) over the YRB. Additionally, Yang et al. (2019) suggested that the ICP soil moisture could be used as one of seasonal predictors of summer extreme high temperature events over the YRB. In this current study, our main objective is to explore the potential effect of the ICP soil moisture in spring on the following summer's YRB precipitation extremes, which may benefit the seasonal predictions of extreme precipitation events over East Asia.

The East Asian monsoon system experienced a climate shift in the early 1990s, with an interdecadal variation of the large-scale circulation background (Ding et al. 2008, 2009). This resulted in changes to the processes affecting summer precipitation over East Asia to a certain extent. For example, before the early 1990s, the summer monsoonal precipitation over the YRB had a strong positive correlation with the western Pacific subtropical high (WPSH) intensity, but then this relationship dramatically weakened (Gao et al. 2015). Therefore, another issue needs to be addressed: How does the effect of the spring ICP soil moisture on the following summer's YRB precipitation extremes vary with a changing climatic background? The findings in this study indicated that the occurrence of summer precipitation extremes over the YRB was strongly linked to the ICP soil moisture anomaly in the preceding spring. Furthermore, an interdecadal change in the effect of the spring ICP soil moisture on the summer YRB precipitation extremes was revealed during our investigations.

The rest of this paper is arranged as follows. Section 2 presents the data and methods. Section 3 examines the features of summer precipitation extremes and the mei-yu front. Section 4 reveals the interdecadal change in the relationship between spring ICP soil moisture and the following summer's YRB precipitation extremes. In section 5, we demonstrate the different effects of the spring ICP soil moisture on the following summer monsoonal circulation, mei-yu front, and YRB precipitation extremes before and after the early 1990s. Section 6 is a summary with a discussion.

2. Data and methods

a. Datasets

The China Meteorological Administration provides a gridded (0.5° × 0.5°) daily observed precipitation dataset (http://data.cma.cn/data/cdcdetail/dataCode/SURF_CLI_CHN_PRE_DAY_GRID_0.5.html), which is collected from more than 2000 stations over mainland China and has been widely used in studies of climate extremes (Ren et al. 2014; Li et al. 2018). The monthly atmospheric fields, including the geopotential height, humidity, air temperature, and horizontal and vertical wind (1.25° × 1.25°), were obtained from the Japanese 55-Year Reanalysis dataset (JRA-55) of the Japan Meteorological Agency (Kobayashi et al. 2015). A monthly sea surface temperature (SST) dataset (1° × 1°) was acquired from the Hadley Centre (Rayner et al. 2003).

For soil moisture, the Global Land Data Assimilation System (GLDAS) produces a long-term dataset (1° × 1°; Rodell et al. 2004), which has been used previously in studies related to East Asia land surface processes (Wu and Zhang 2013; Cheng et al. 2015). The GLDAS V2.0 dataset was adopted in this study, and it was produced by the National Centers for Environmental Prediction–Oregon State University–Air Force–Hydrologic Research Laboratory (Noah) land surface model (Ek et al. 2003) with the meteorological forcing datasets provided by Princeton University (Sheffield et al. 2006). The soil moisture information for the top layer (0–10 cm) was used in this study, due to its direct feedbacks on the atmosphere (Dirmeyer 2011). The top layer soil temperature was also used as the surface temperature to represent the land surface thermal state. The study period was set from 1961 to 2010 because there were data available for this period in all datasets. Besides, a monthly global observed precipitation dataset (0.5° × 0.5°) provided by the Climatic Research Unit (CRU) at the University of East Anglia was used to check the relationship between spring soil moisture over the ICP and summer precipitation extremes over the YRB for the period including the recent eight years (1961–2018).

The seasonal means were based on 3-month averaged data: spring (March–May), summer (June–August), and winter (December–February). For the synoptic-scale analyses, we further adopt the ERA-Interim daily reanalysis dataset (including wind, temperature, and geopotential height fields with a horizontal resolution of 2.5° × 2.5° for the period of 1979–2010) provided by the European Centre for Medium-Range Weather Forecasts (ECMWF).

b. Methods

In this study, precipitation extremes were defined as daily precipitation exceeding 50 mm, which is considered to represent precipitation intense enough to affect human activities and cause floods by the Chinese operational meteorological services (Chen and Zhai 2013). The 50 mm day^{-1} threshold exceeded the 95th percentile of precipitation at most (90%) Chinese ground observation stations during the warm season (Chen and Zhai 2013). When the threshold of precipitation extremes was defined as daily precipitation exceeding 40 or 60 mm, the final results were almost the same. Therefore, in this study, the occurrence of precipitation extremes in each grid were described in terms of the number of days with precipitation exceeding 50 mm within a given period.

In addition, the tropospheric water vapor flux and its divergence were vertically integrated from 300 to 1000 hPa because there is little moisture above 300 hPa. The equation used was as follows:

$$Q = \frac{1}{g}\int_{P_t}^{P_s} \nabla \cdot (q\mathbf{V})\, dP, \tag{1}$$

where g, q, $\mathbf{V}$, and P are the gravitational acceleration, specific humidity, horizontal wind velocity, and air pressure, respectively. The terms P_t and P_s denote the top (300 hPa) and surface (1000 hPa) pressure layers, respectively. A value of $Q > 0$ indicates the divergence of water vapor transport.

Generally, precipitation extremes are associated with abnormal ascent in the troposphere. Thus, the omega equation was employed to diagnose the vertical motion in our study. The equation was as follows:

$$\sigma\left(\nabla^2 + \frac{f_0^2}{\sigma}\frac{\partial^2}{\partial p}\right)\omega = f_0\frac{\partial}{\partial p}\left[\mathbf{V}_g \cdot \nabla\left(\frac{1}{f_0}\nabla^2\phi + f\right)\right] + \nabla^2\left[\mathbf{V}_g \cdot \nabla\left(-\frac{\partial\phi}{\partial p}\right)\right] - \frac{k}{p}\nabla^2 J, \tag{2}$$

where all symbols have their conventional meanings in meteorology [see Holton (2004) for detailed information]. The left term (hereafter term A) is proportional to $-\omega$ (or w). The other three terms on the right are physical processes contributing to the vertical motion: the vertical gradient of absolute vorticity advection (hereafter term B), temperature advection (hereafter term C), and diabatic heating (hereafter term D). Normally, the diabatic heating (term D) is a relatively small term (Feng et al. 2014), thus only the terms of vorticity advection (term B) and temperature advection (term C) (adiabatic processes) were considered in this study. According to Eq. (2), a positive vertical gradient of absolute vorticity advection or a warm temperature advection is conductive to forming and maintaining the ascent.

A regression approach was used for the calculation of removing the SST anomaly signals:

$$V = V^* - S \times \mathrm{cov}(V^*, S)/\mathrm{var}(S), \tag{3}$$

where V^* is a given variable, S is the regional averaged SST anomaly, $\mathrm{cov}(V^*, S)$ is the covariance between the variable and the SST anomalies, $\mathrm{var}(S)$ is the variance of the SST anomaly, and V is the variable after removing the SST anomaly.

Our study was mainly based on the correlation and regression analyses. For their statistical significance, we used $p < 0.1$, 0.01, and 0.001 to denote the results significantly exceeding the 90%, 99%, and 99.9% confidence levels, respectively.

c. Model simulations

To further support our conclusion from statistics that the ICP heating could affect the WPSH, we designed a set of numerical experiments using a full-physics atmospheric general circulation model (AGCM) ECHAM v4.6 (Roeckner et al. 1996) at T42 horizontal resolution. In addition to the control run (CTRL) that was forced by the monthly climatological SST field, the heating forcing in the ICP region with a vertically decreased rate with height was prescribed in the sensitivity experiments. Specifically, in the CTRL experiment, the AGCM was integrated for 40 years, and results from the last 20 years were analyzed. We then conducted 20 members of sensitivity experiments, each of which was integrated for 1 year and the integration starts from 1 January but with different initial conditions. In the sensitivity experiments, the three-dimensional heating anomalies are added to the original heating rate in the temperature equation at every time step in spring; the specific heating forcing at surface has an oval structure and decreases with height as in reality (its magnitude gradually decreases from surface to 400 hPa and becomes marginal above 400 hPa). Finally, the differences between the multimember ensemble from the sensitivity experiments and the CTRL experiment are used to confirm that the ICP heating can affect the geopotential height anomaly and associated circulations. It is worth mentioning that this AGCM (ECHAM4.6) has been widely used in previous studies (e.g., Wang and Chen 2017; Wang and Li 2020) and the sensitivity experiment with a prescribed heating forcing has also been applied in recent studies (e.g., Xiang et al. 2014; Wang et al. 2017, 2018).

3. Summer precipitation extremes and the mei-yu front

The climatology of the occurrence of summer precipitation extremes over eastern China is shown in Fig. 1a. There were two regions that exhibited a relatively large number of precipitation extremes during 1961–2010: the southeast coastal areas of China and the YRB. In the past five decades, the occurrence of extreme events over some parts of those two regions exceed 2 days on average in the summer. Both regions displayed a relatively larger interannual variability (Fig. 1b). The maximum standard deviation of the occurrence of precipitation extremes in summer was approximately 2 days. This indicates that the southeastern coastal areas and the YRB are prone to intense precipitation in summer.

While the frequent summer precipitation extremes in southeast coastal areas are largely due to frequent tropical cyclones (Wen et al. 2007), the frequent summer precipitation extremes over the YRB might be associated with a strong mei-yu front (Cen et al. 2015; Chen and Zhai 2016). Accompanied by the upward movement of warm and wet air, the mei-yu front favors the occurrence of precipitation extremes. Because wet-warm and dry-cold air masses can be respectively characterized by a relatively high and low equivalent potential temperature θ_e (determined by both temperature and humidity), the mei-yu front can feature a relatively large meridional θ_e gradient ($-d\theta_e/dy$) in the lower troposphere across the YRB (Li and Lu 2017; Gao et al. 2019). Therefore, as Fig. 1c shows, a band with a large climatic meridional θ_e gradient ($-d\theta_e/dy$) at 700 hPa covers the YRB during summer, and can be used to indicate the intensity of the mei-yu front. Moreover, the largest variability of the θ_e gradient is also located in the YRB (Fig. 1d). This implies that a strong summer mei-yu front over the YRB is accompanied by frequent occurrences of local precipitation extremes.

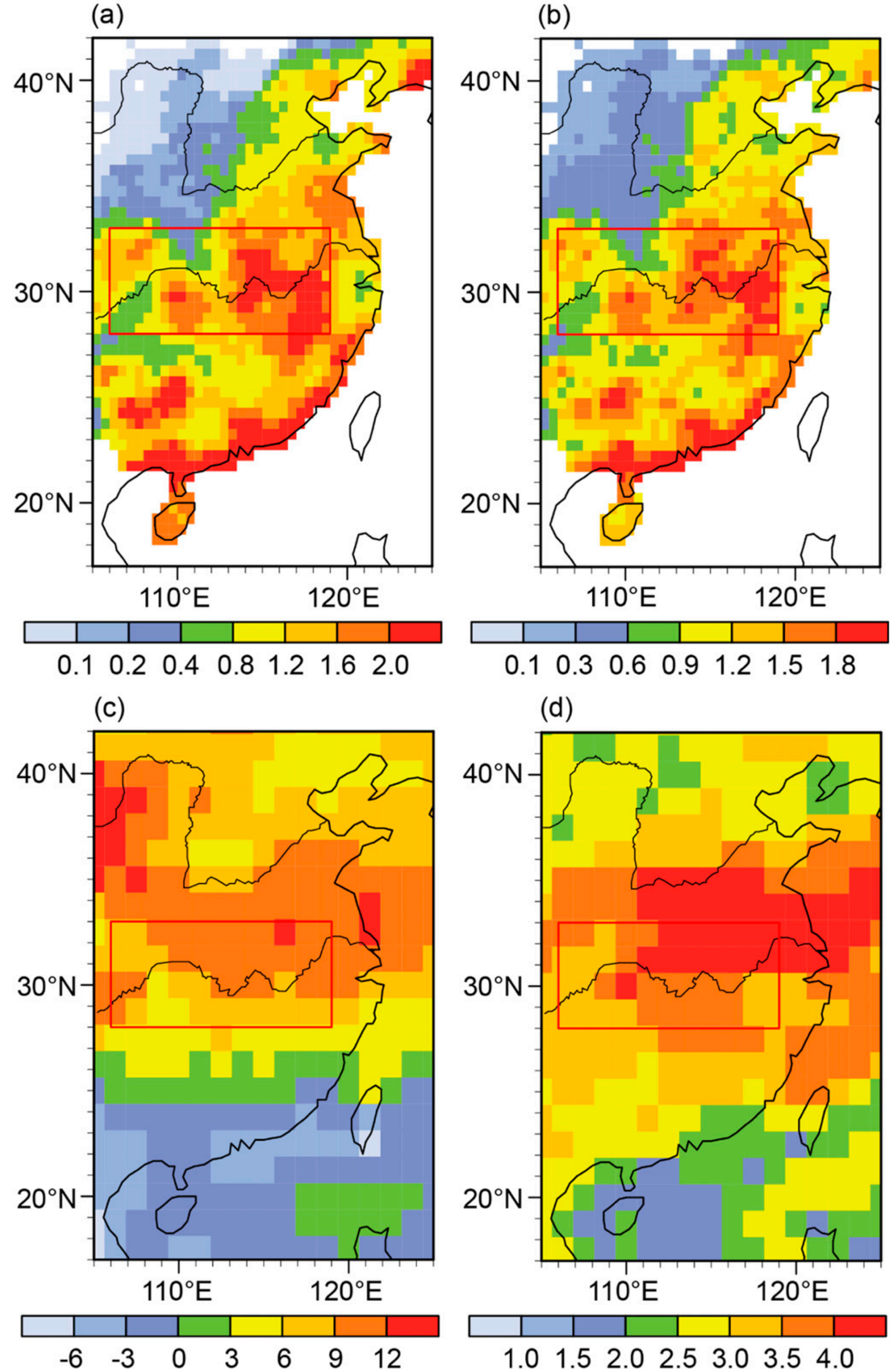

FIG. 1. (a) Climatic mean and (b) standard deviation of the occurrences of summer precipitation extremes during 1961–2010 (day). (c),(d) As in (a) and (b), but for the meridional θ_e gradient ($-d\theta_e/dy$; 1×10^{-6} K m^{-1}) at 700 hPa. The red boxes denote the Yangtze River basin (YRB; 106°–119°E, 28°–33°N).

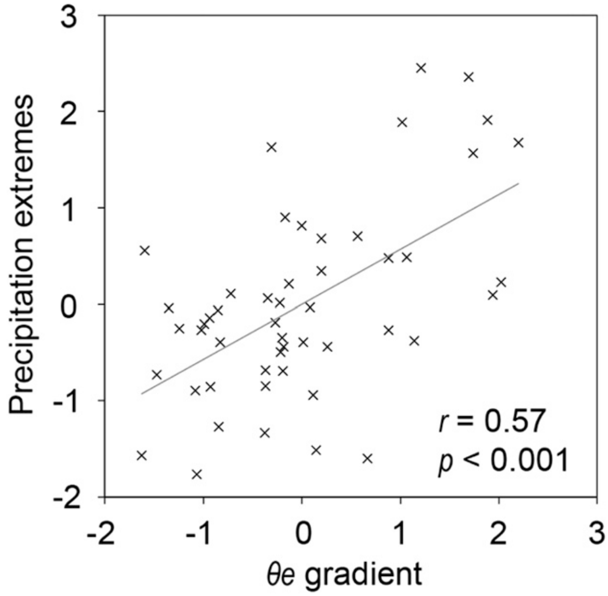

FIG. 2. Scatterplot between the 700-hPa $-d\theta_e/dy$ and occurrence of precipitation extremes averaged over the Yangtze River basin in summer during 1961–2010. All data were linearly detrended and standardized for the correlation analysis.

Figure 2 demonstrates the relationship between the number of summer precipitation extremes and the regionally averaged mei-yu front strength over the YRB (106°–119°E, 28°–33°N). As expected, the correlation coefficient was high at 0.57, which was statistically significant at $p < 0.001$. This confirms that a strong mei-yu front would favor more occurrences of summer precipitation extremes over the YRB. Previous studies have documented that the precipitation extremes are intense frontal processes, which are closely related to the strong ascent of warm-wet air along a quasi-stationary front at the synoptic scale (Ninomiya and Shibagaki 2007; Chen and Zhai 2015). Here, our result showed that the seasonal mean states of the mei-yu front intensity also have great implications on the frequency of summer precipitation extremes over the YRB.

Figure 3 shows the atmospheric states associated with a stronger mei-yu front in terms of the correlations of the water vapor flux and vertical velocity with the front intensity. The monsoonal southwesterly wind brings warm and moist air to the YRB where it meets the cold and dry air over the north, forming the mei-yu front. Thus, a strong mei-yu front is accompanied by large amounts of warm-wet air moisture transported to YRB in summer (Fig. 3a). In addition, a strong mei-yu front is linked to a strong upward movement (Fig. 3b). Intense precipitation is always related to the strong ascent of the warm and wet air along a quasi-stationary front (Ninomiya and Shibagaki 2007). Therefore, a strong air moisture convergence along with a strong upward movement could provide favorable conditions for summer precipitation extremes over the YRB (Fig. 2).

In addition, we adopted the omega equation to diagnosis the maintenance mechanisms of the abnormal upward movement

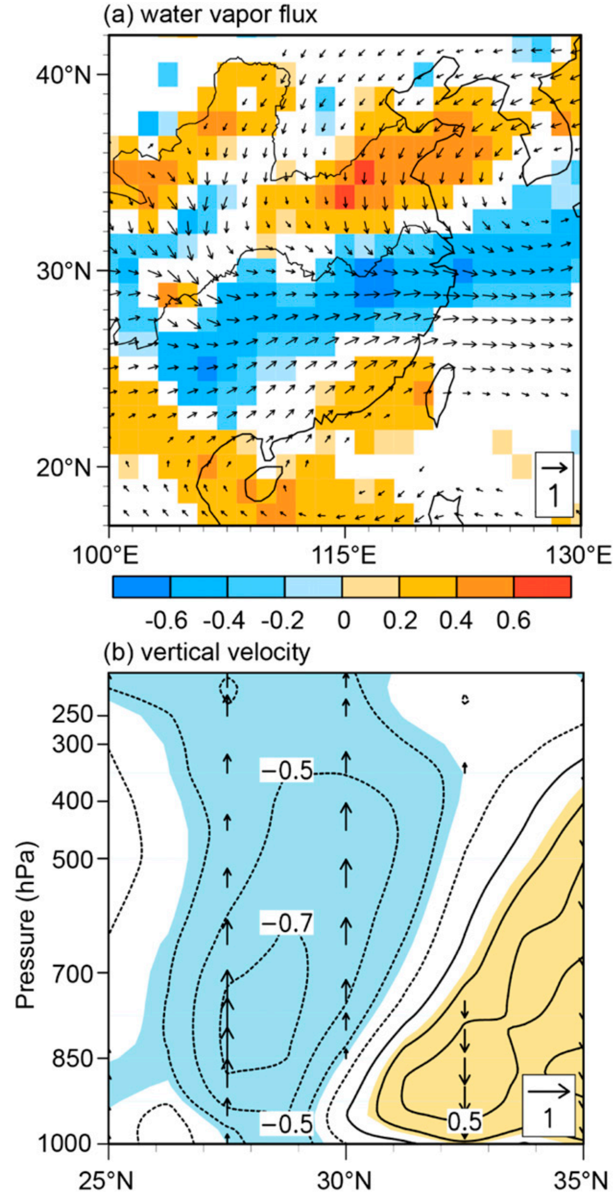

FIG. 3. (a) Correlation coefficients for the relationship of water vapor flux (arrows; only arrows significant at $p < 0.1$ are shown) and its divergence (color; only areas significant at $p < 0.1$ are colored) anomalies integrated from 300 to 1000 hPa with the $-d\theta_e/dy$ averaged over the Yangtze River basin in summer during 1961–2010. (b) Correlation coefficients between the vertical velocity anomaly (contours, the arrows denote the direction) averaged over 106°–119°E and the $-d\theta_e/dy$ averaged over the YRB in summer during 1961–2010. The colored areas are significant at $p < 0.1$. All data were linearly detrended and standardized for the correlation analysis.

related to the occurrence of the YRB precipitation extremes in summer. Based on Eq. (2), the major contributions to the vertical motion (term A) are the vertical gradient of absolute vorticity advection (term B) and the temperature advection (term C). First, the upward movement (positive term A)

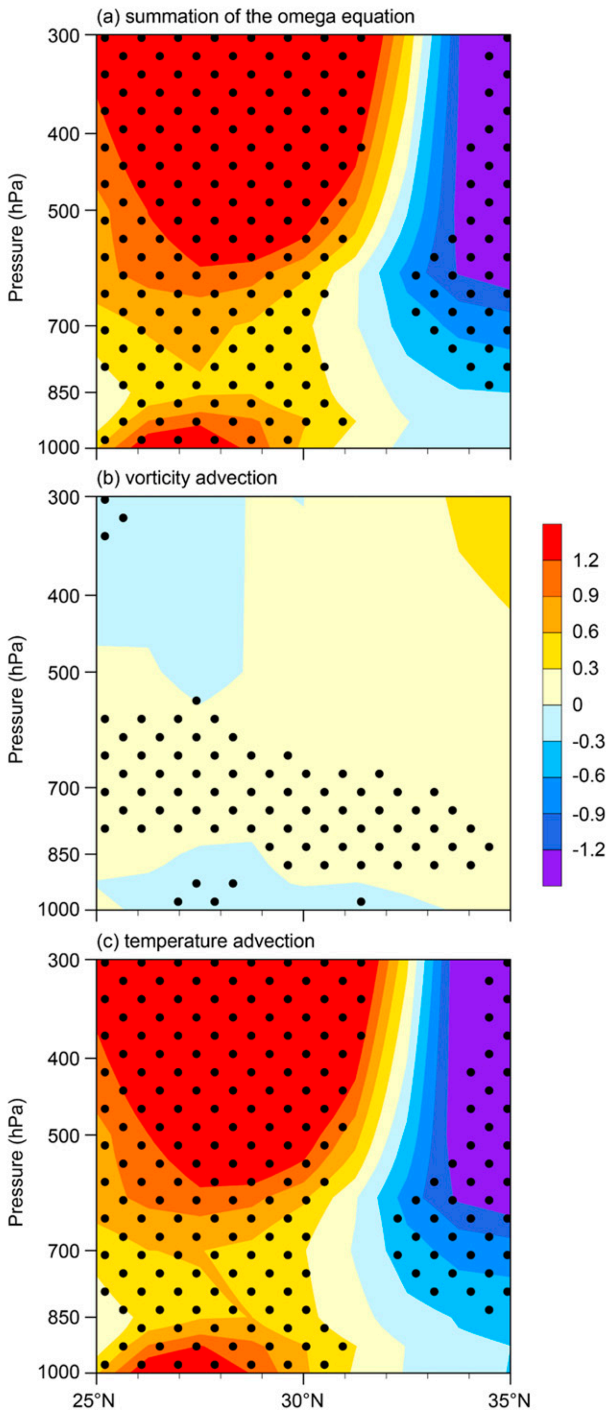

FIG. 4. Regression of the (a) term A, (b) term B, and (c) term C anomalies (1×10^{-16} m s^{-1} kg^{-1}) in the omega equation averaged over 106°–119°E with respect to the standardized occurrence of precipitation extremes averaged over the YRB in summer during 1961–2010. The dotted areas were significant with $p < 0.1$.

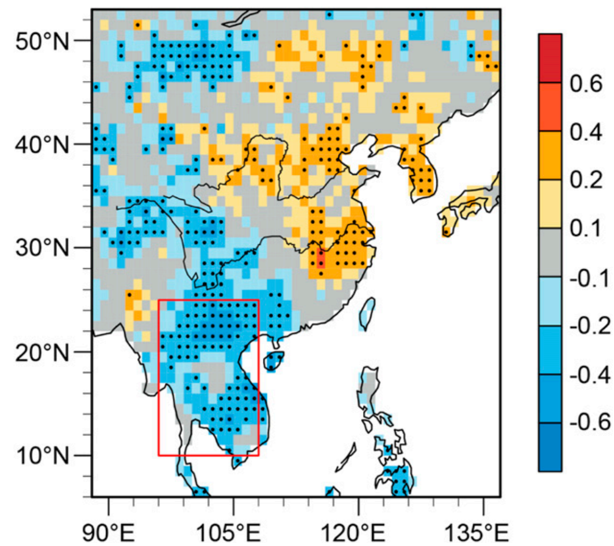

FIG. 5. Correlation coefficients for the relationship of the spring soil moisture anomaly with the occurrence of summer precipitation extremes averaged over the YRB during 1961–2010. The dotted areas are significant at $p < 0.1$. The red box denotes the Indo-China Peninsula (ICP; 96°–108°E, 10°–25°N). All data were linearly detrended and standardized for the correlation analysis.

related to the YRB precipitation extremes mainly dominated the YRB region in summer (Fig. 4a), confirming that the summer with stronger ascending motion had more precipitation extremes over the YRB. Figures 4b and 4c further illustrated the YRB precipitation extremes–related term B and term C anomalies in Eq. (2). It was obvious that the vertical motion related to the YRB precipitation extremes is mainly maintained by the term C, while the term B anomaly is much weaker. Therefore, the abnormal warm–wet air transporting to the YRB induces the mei-yu front and local vertical motion anomalies in summer, resulting in frequent occurrences of precipitation extremes.

4. The weakening relationship between spring soil moisture over the ICP and summer precipitation extremes over the YRB

Gao et al. (2019) revealed that the soil moisture anomaly over the ICP in spring can affect the East Asian monsoonal circulation, resulting in abnormal climatic states over the YRB in summer. It is possible that such a soil moisture anomaly might also affect summer precipitation extremes over the YRB. Figure 5 shows the distribution of correlation coefficients for the relationship between spring soil moisture over East Asia and the number of summer extreme precipitation events averaged over the YRB during 1961–2010. A large area of negative values dominated the ICP, which indicated that summer precipitation extremes over the YRB would occur more frequently when the ICP soil was drier than normal in the preceding spring, and vice versa.

The regionally averaged anomalies of spring soil moisture over the ICP (96°–108°E, 10°–25°N) and summer precipitation extremes over the YRB during 1961–2010 are shown in Fig. 6a. The anomalies were generally in the opposite phase in each year, with a correlation coefficient of -0.41 ($p < 0.01$) during the five decades. However, we also identified an instability

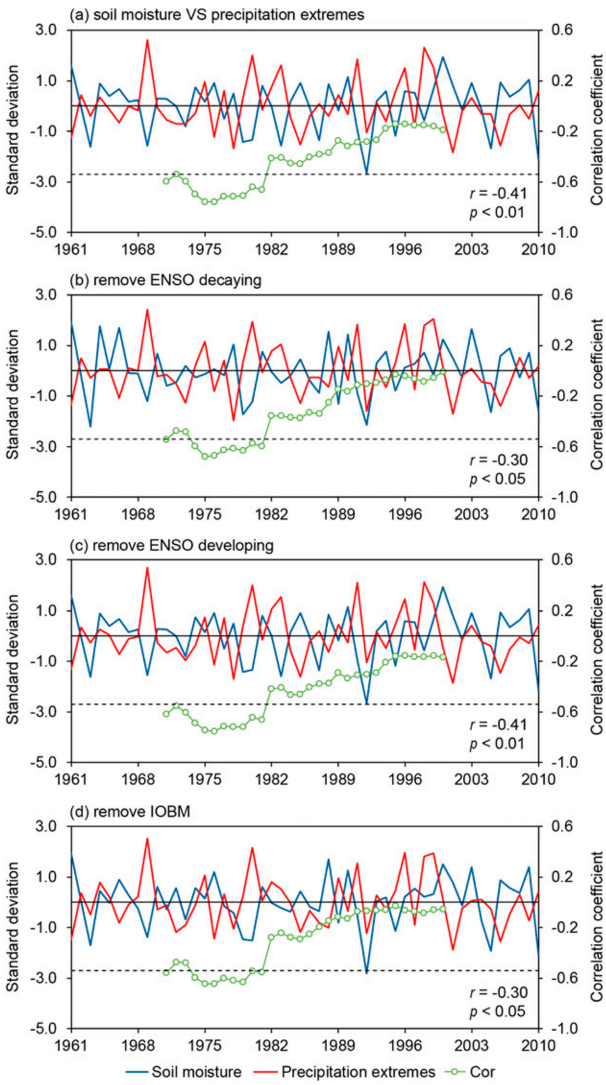

FIG. 6. (a) Interannual anomalies of spring soil moisture averaged over the Indo-China Peninsula and summer precipitation extremes averaged over the Yangtze River basin. The term r is the correlation coefficient for the period of 1961–2010. The green line with circles is the 21-yr moving correlation coefficient, and the dashed line denotes a significance level of $p < 0.1$. (b)–(d) As in (a), but after the removal of ENSO decaying, developing, and Indian Ocean basin mode (IOBM) signals, respectively. All data were linearly detrended and standardized.

within the negative relationship. The 21-yr moving correlation coefficient was statistically significant until 1981 (the result for the period of 1971–91). The correlation exhibited an interdecadal abrupt change and was not statistically significant in recent decades (1992–2010). This suggests a weakening relationship between the spring ICP soil moisture and the summer YRB precipitation extremes since the early 1990s.

Intense summer precipitation over the YRB is usually connected to tropical SST anomalies, especially El Niño–Southern Oscillation (ENSO) events and associated Indian Ocean basin (40°–100°E, 20°N–20°S) SST anomalies [the Indian Ocean basin mode (IOBM)]. The ENSO and IOBM events have important roles in regulating the East Asian summer monsoon circulation, and thus affect the monsoonal precipitation (Xie et al. 2016; Zhang et al. 2016). ENSO SST anomalies reach their peak in boreal winter. Thus, the ENSO events usually undergo their developing and decaying stages in the preceding and following summers, respectively, resulting in evident climatic effects on monsoon circulations (Xie et al. 2009; Wen et al. 2018). Besides, the IOBM events are usually strong in summer, sustaining such effects of ENSO (Tao et al. 2016; Xie et al. 2016). Therefore, we calculated the previous and subsequent winter SST anomalies in the Niño-3.4 region (120°–170°W, 5°N–5°S) as the ENSO decaying and developing signals, and the simultaneous summer SST anomalies in the Indian Ocean basin as the IOBM signal. Figures 6b–d show the results after removing those signals. After excluding the influences of the SST anomalies, the negative relationships between the spring ICP soil moisture and the summer YRB precipitation extremes anomalies were still statistically significant for the whole study period. This suggests that the effects of the spring ICP soil moisture anomaly on the summer YRB precipitation extremes were independent of the SST forcing. More importantly, the decadal weakening identified from the 21-yr moving correlation was also reproduced in each case.

Figure 7 shows the distribution of the correlation coefficient for the relationship between the frequency of summer precipitation extremes over eastern China with the preceding spring soil moisture anomaly averaged over the ICP. Precipitation extremes over the YRB exhibited a relatively strong connection to the ICP soil moisture, with significant negative correlation coefficients of over -0.20 ($p < 0.1$) during the past five decades (Fig. 7a). Considering the interdecadal changes reflected by the 21-yr moving correlation, we divided the study period into two subperiods: 1961–91 and 1992–2010. During the early period, the negative correlation over the YRB was even stronger than that for the whole period (Fig. 7b). During the period after 1991, there was a weaker correlation of summer precipitation extremes with the spring ICP soil moisture anomalies in the YRB (Fig. 7c). This further implies that the influence of the ICP soil moisture in spring on the following summer YRB precipitation extremes has undergone an interdecadal weakening.

5. Interdecadal changes in the effects of the spring ICP soil moisture

A major mechanism by which the ICP soil moisture affects the East Asian summer climate is its thermal control, along with the strong persistence of anomalies (Gao et al. 2019). First, the precipitation changes have always been considered as the primary causes for the soil moisture anomalies (Piao et al. 2009). As we expected, the correlation coefficient between local precipitation and soil moisture anomalies averaged over the ICP in spring was 0.82 ($p < 0.001$) during 1961–2010 (figure not shown). Unlike precipitation anomaly that induced by the rapidly changes of the atmospheric circulations, soil moisture anomaly has a strong memory. Figure 8 shows the correlations of monthly precipitation and soil moisture averaged over the ICP with their mean spring states during 1961–2010. Apparently,

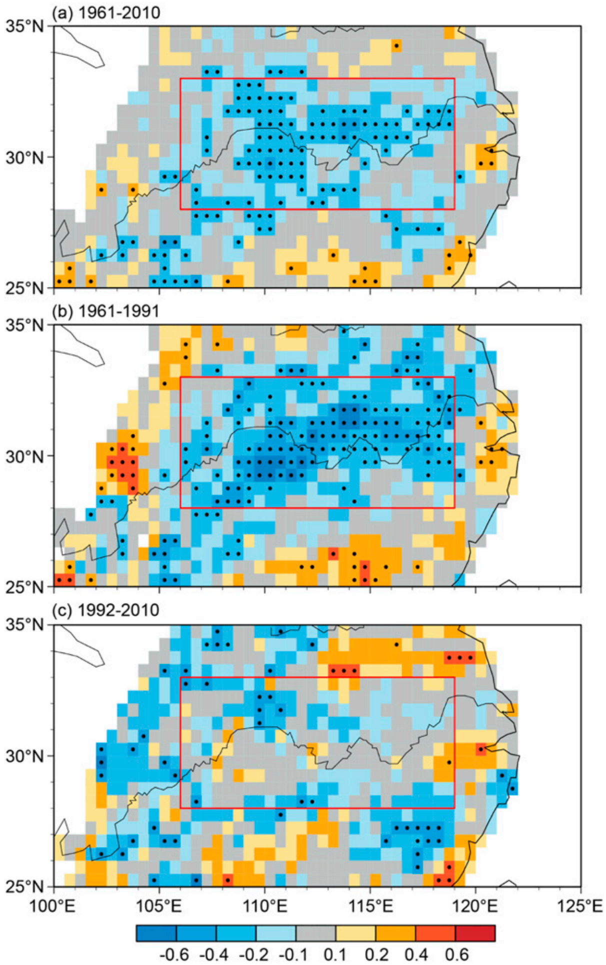

FIG. 7. (a) Correlation coefficients for the relationship between the occurrence of summer precipitation extremes and the spring soil moisture anomaly averaged over the Indo-China Peninsula for the period of 1961–2010. The dotted areas are significant at $p < 0.1$. The red box denotes the Yangtze River basin. (b),(c) As in (a), but for the periods of 1961–91 and 1992–2010, respectively. All data were linearly detrended and standardized for the correlation analysis.

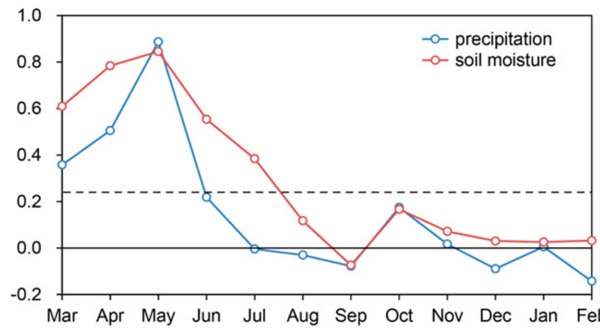

FIG. 8. Correlation coefficients of monthly precipitation and soil moisture anomalies with their spring anomalies averaged over the ICP for the period of 1961–2010. The dashed line denotes the significance level of $p < 0.1$. All data were linearly detrended.

precipitation anomalies had little connection between in spring and summer, while spring soil moisture anomalies exhibited strong positive correlations ($p < 0.1$) with their changes in summer (mainly in June and July). In general, soil moisture anomalies could be sustained for weeks or even months, and thus continuously regulate the surface temperature by constraining the surface evapotranspiration. For example, an abnormally lower soil moisture reduces evapotranspiration, and then increases the local temperature. As a result, the continuous abnormal surface heating affects the state of the atmosphere, causing variations of the circulation system (Zuo and Zhang 2016; Gao et al. 2019). It was found that the local thermal effects of soil moisture over the ICP were similar during the two subperiods, but the resultant responses of the East Asian summer monsoonal circulation and mei-yu front were distinctly different.

Figure 9 shows the responses of local surface temperature to the spring ICP soil moisture anomalies. For the period of 1961–91, the simultaneous surface temperature could rise up by over 0.2–0.4 K if the soil moisture was abnormally lower than usual by -1 standard deviation in spring over the ICP (Fig. 9a). Moreover, this anomalously stronger heating could be sustained in summer by a temperature increase of more than 0.1 K on average (Fig. 9c), and vice versa. This indicates that the ICP soil moisture could induce a change in surface thermal conditions. The responses of the local surface temperatures in spring and summer were basically the same in the recent period (1992–2010; Figs. 9b,d).

Theoretically, an abnormally higher temperature on the land surface heats the air column, and thus increases the geopotential height (Fischer et al. 2007). As shown in Fig. 10a, the 500-hPa geopotential height was significantly uplifted by over 4 gpm over the ICP when the local soil moisture was -1 standard deviation lower than usual in spring during 1961–91. Under such conditions, the abnormal center of the geopotential height exhibited an east–west band distribution from the western Pacific Ocean to the ICP. The 5860-gpm contour was used to denote the WPSH. It was evident that the WPSH extended westward in association with a lower ICP soil moisture. In 1992–2010, the effect of a similar abnormal surface heating on summer geopotential height over the ICP was weaker by 2 gpm (Fig. 10b). The geopotential height anomaly center extended northwestward to southern China. Accordingly, the anomalous WPSH tended to be located toward the south and the accompanying westward extension was far less obvious. This indicates that the effects of the abnormal thermal conditions induced by the ICP soil moisture anomaly on the large-scale atmospheric circulation have changed between the two subperiods. This may be because the East Asian summer monsoon system has experienced an abrupt climate shift, with an interdecadal westward extension of the climatological WPSH around the early 1990s (Ding et al. 2009). Therefore, different responses of the large-scale monsoonal circulation and mei-yu front anomalies to the identical surface heating over the ICP should be expected under different settings of the climatological monsoonal circulation.

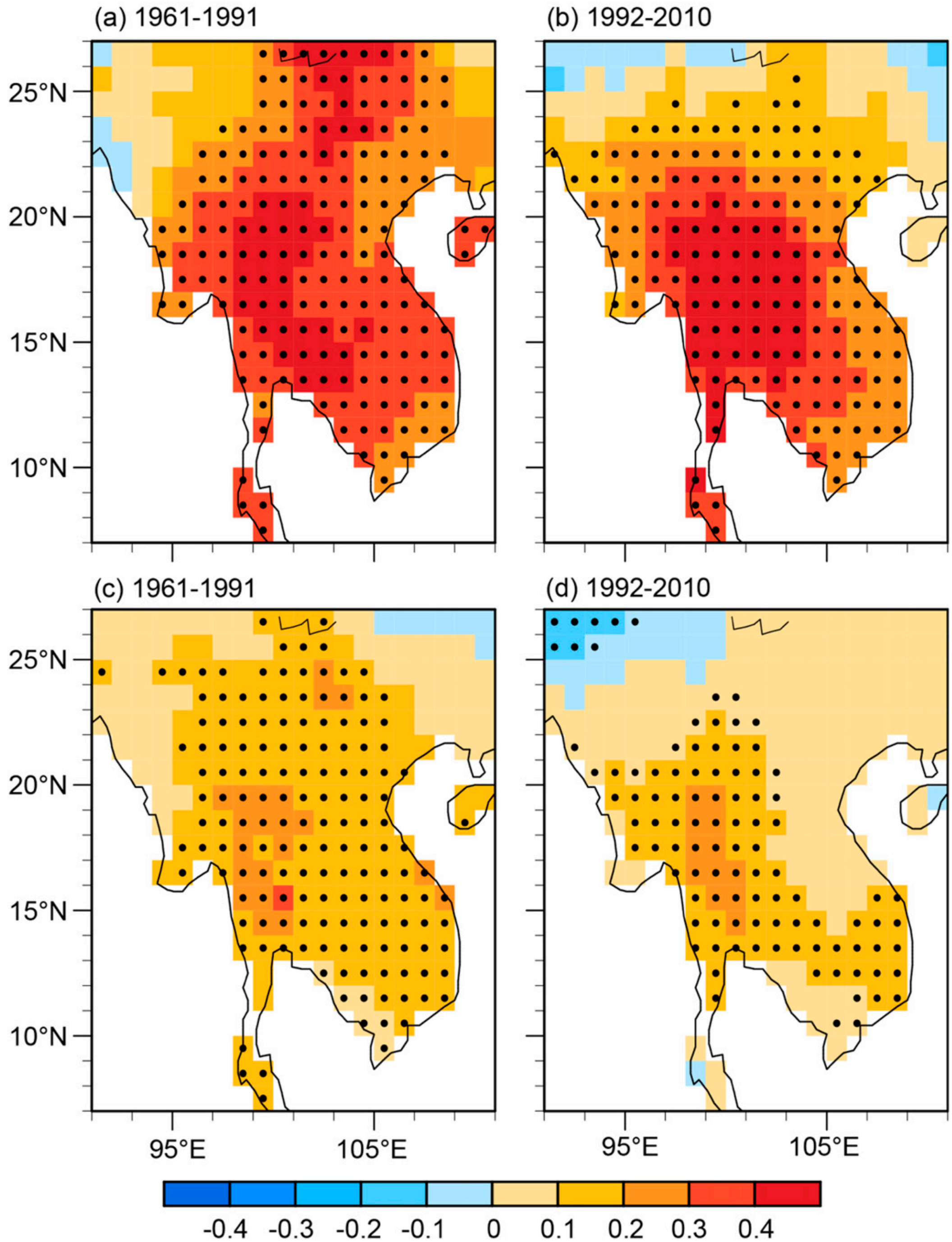

FIG. 9. Regressions of (a) spring and (c) summer surface temperature anomalies (K) with respect to the negative standardized spring soil moisture averaged over the Indo-China Peninsula during 1961–91. The dotted areas were significant at $p < 0.1$. (b),(d) As in (a) and (c), but for the period of 1992–2010. All data were linearly detrended for the regression analysis.

To verify the above findings about the abnormal ICP heating affecting the WPSH, a set of numerical experiments was designed using an AGCM. Figure 11a shows the mean state of summer 500-hPa geopotential height in the control run and the anthropogenic surface heating forcing area. The 5910-gpm contour could denote the shape of the WPSH in summer, and the location and magnitude of the spring surface heating forcing were mainly based on Fig. 9. In the sensitively experiments, summer geopotential height over the ICP was uplifted, and the WPSH was extended westward (Fig. 11b). The

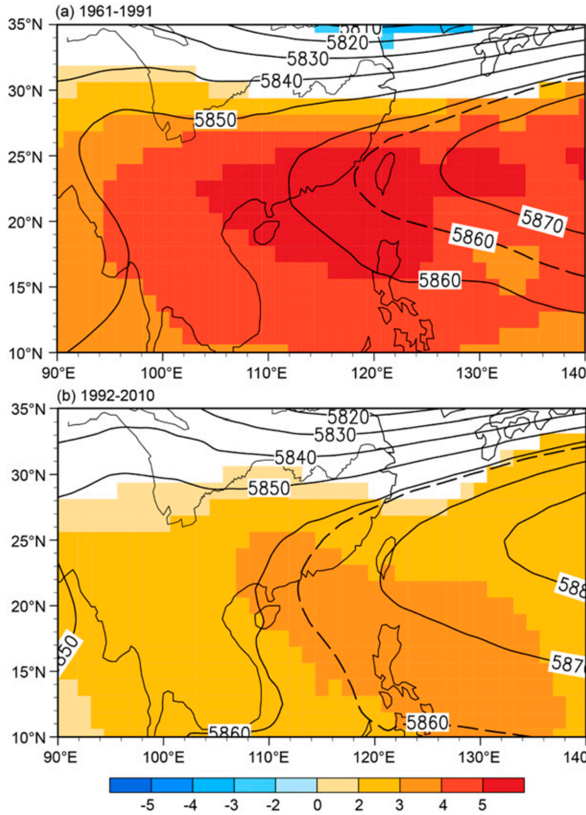

FIG. 10. Regression of the summer 500-hPa geopotential height (colors; gpm) anomaly with respect to the negative standardized spring soil moisture anomaly averaged over the Indo-China Peninsula during (a) 1961–91 and (b) 1992–2010. Only the areas of the geopotential height anomaly exceeding the significance level of $p < 0.1$ are shaded with colors. The contours are the sums of the climatic means plus the regression anomalies of the geopotential height for the two periods. The dashed lines denote the climatic means of the 5860-gpm contour in the two periods. All data were linearly detrended for the regression analysis.

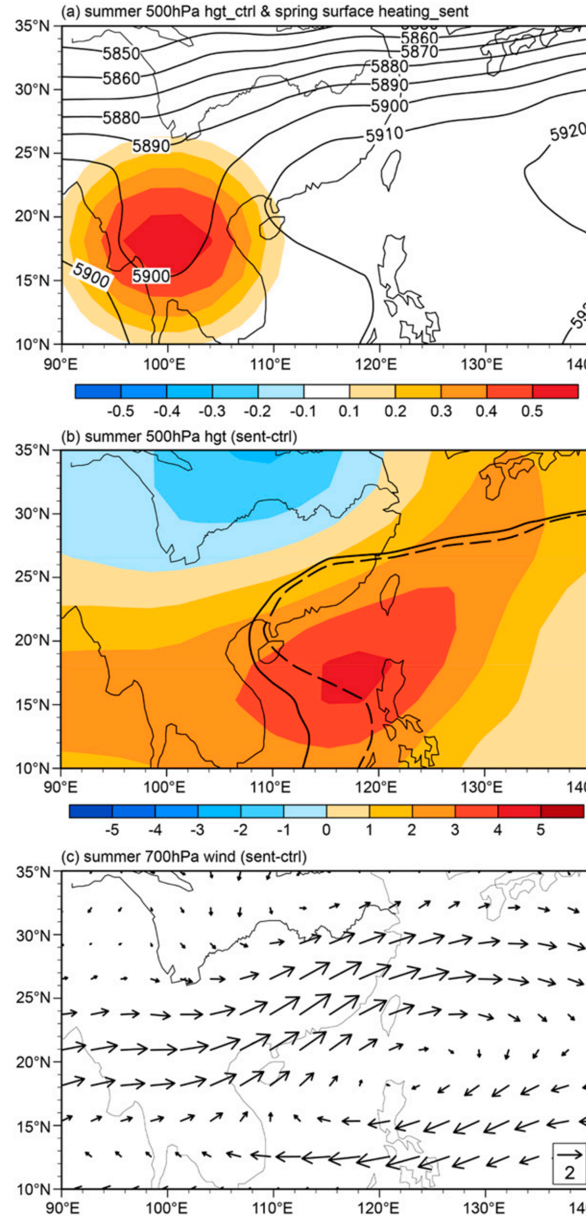

FIG. 11. (a) The mean 500-hPa geopotential height (contours; gpm) in summer in the control run, and the anthropogenic surface heating forcing (colors; K) in spring in the sensitivity experiments. (b) Difference of summer 500-hPa geopotential height (colors; gpm) between the sensitivity experiments and the control run (sensitivity minus control), and the solid and dashed lines denote the means of 5910-gpm contour in the sensitivity experiments and the control run. (c) Difference of summer 700-hPa wind ($\mathrm{m\,s^{-1}}$) between the sensitivity experiments and the control run (sensitivity minus control).

difference pattern was similar to Fig. 10, which confirmed that the abnormal heating induced by the spring ICP soil moisture could contribute to the WPSH shifting zonally.

The WPSH is one of the key components of the East Asian summer monsoon system, and variations in its strength and shape evidently adjust the monsoonal wind and water vapor flux. Figure 12 shows the response of the 700-hPa wind and vertically integrated water vapor flux anomalies to the abnormal spring ICP soil moisture. Similar to the 500-hPa geopotential height anomaly, the 700-hPa geopotential height anomaly center also extended westward to the ICP land surface in the early subperiod (Fig. 12a). An abnormal anticyclonic pattern of the wind field occurred along the western rim of the anomaly center, leading to an enhanced southwesterly monsoonal wind over southern China. This was also verified in our numerical experiments: the 700-hPa wind also exhibited a strengthened southwesterly wind over the southern China in the sensitivity experiments (Fig. 11c). Correspondingly, the strengthened wind brought excessive moisture to the YRB, causing an evident local water vapor convergence (Fig. 12c). This would favor mei-yu front precipitation over the YRB in summer. In comparison, the abnormal wind and water vapor flux fields responding to the

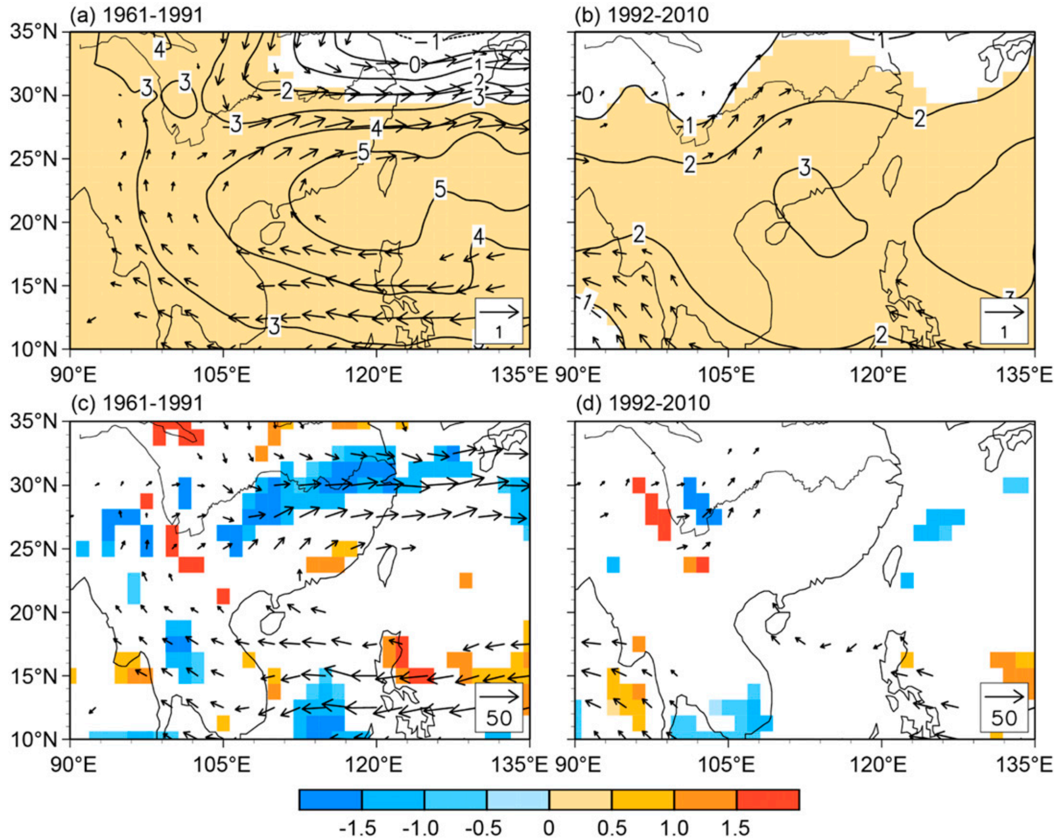

FIG. 12. Regressions of the summer 700-hPa geopotential height (contours; gpm; the shaded areas were significant at $p < 0.1$) and wind (arrows; m s^{-1}; the arrows were significant with $p < 0.1$) anomalies with respect to the negative standardized soil moisture anomalies averaged over the Indo-China Peninsula during (a) 1961–91 and (b) 1992–2010. (c),(d) As in (a) and (b), but for the water vapor flux (arrows; kg m^{-1} s^{-1}; only arrows significant at $p < 0.1$ are shown) and its divergence (colors; 1×10^5 kg m^{-2} s^{-1}; only areas significant at $p < 0.1$ are colored) anomalies. All data were linearly detrended for the regression analysis.

spring ICP soil moisture anomaly were insignificant over southern China, with a relatively weaker uplifted 700-hPa geopotential height during 1992–2010 (Figs. 12b,d).

The monsoonal circulation anomaly not only generated abnormal water vapor transport to the YRB, but also affected the mean state of the mei-yu front during summer. As shown in Fig. 13a, in the early subperiod, an excessive transport of the warm and wet air masses over southern China increased the local θ_e, which led to an anomalously larger meridional θ_e gradient across the YRB. This indicates that the strengthened southwesterly monsoon induced by the drier ICP surface in spring resulted in an enhanced mei-yu front in summer, which also benefited the ascending motion over the YRB. Precipitation extremes are more likely to occur under these circumstances. In contrast, the weakened responses of monsoonal circulation resulted in fewer changes of the mei-yu front over the YRB during the summer of 1992–2010 (Fig. 13b).

The above findings indicate that the thermal control of the ICP soil moisture influenced the East Asian summer monsoon circulation, and thus affected the mean state of the mei-yu front before the early 1990s. Furthermore, the occurrence of summer precipitation extremes over the YRB was strongly associated with the mei-yu front. Figure 14 shows the relationships among the spring ICP soil moisture, the mei-yu front intensity, and the summer YRB precipitation extremes, which can be used to better understand the occurrence of summer precipitation extremes over the YRB. In the early period (1961–91), the ICP soil moisture had a strong negative relationship with the mei-yu front intensity (Fig. 14a), and the mei-yu front intensity had a significant ($p < 0.001$) positive correlation with the YRB precipitation extremes (Fig. 14c). Therefore, the spring ICP soil moisture exerted a strong influence on the frequency of summer YRB precipitation extremes, with a negative correlation coefficient of -0.63 (Fig. 14e). In contrast, during the recent decade (1992–2010), the effect of the ICP soil moisture anomaly on the mei-yu front was dramatically weakened, which was reflected by an insignificant correlation coefficient of -0.07 (Fig. 14b), whereas the connection between the mei-yu front intensity and the YRB precipitation extremes in summer was still robust (Fig. 14d). As a result, ICP soil moisture had an insignificant influence on the occurrence of YRB precipitation extremes (Fig. 14f).

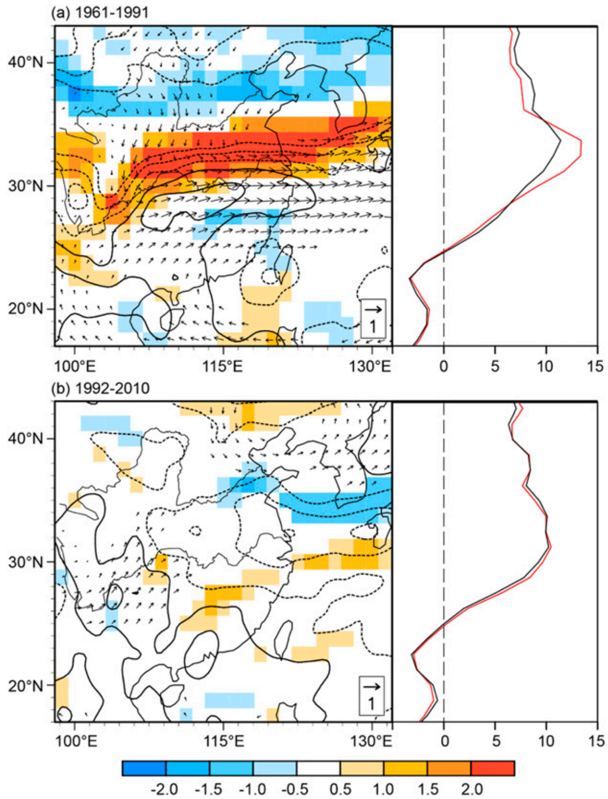

FIG. 13. Regressions of the summer 700-hPa θ_e (contours; K), $-d\theta_e/dy$ (colors; $1 \times 10^{-6}\,\mathrm{K\,m^{-1}}$), and wind (arrows; $\mathrm{m\,s^{-1}}$) anomalies with respect to the negative standardized spring soil moisture anomalies averaged over the Indo-China Peninsula during (a) 1961–91 and (b) 1992–2010. Only the areas of the $-d\theta_e/dy$ and wind anomalies exceeding the significance level of $p < 0.1$ are shown with colors and arrows, respectively. The right-hand panels show the corresponding climatic means (black lines) and sums (red lines) of climatic means plus the regression anomalies of the $-d\theta_e/dy$ averaged over 106°–119°E in the two periods. All data were linearly detrended for the regression analysis.

To verify whether the background signals (slow-varying general circulation) or synoptic signals (fast-varying perturbations) dominate the occurrence of the summer YRB precipitation extremes, we decomposed the anomalous temperature advection into the following three terms (Feng et al. 2014):

$$(-\mathbf{V}\cdot\nabla T)' = -\overline{\mathbf{V}}\cdot\nabla T' - \mathbf{V}'\cdot\nabla\overline{T} - \mathbf{V}'\cdot\nabla T', \qquad (4)$$

where a bar denotes the summer mean state of each year, and a prime denotes the daily departure from the mean state. The three terms on the right side of Eq. (4) represent anomalous temperature advection by climatologic mean wind (hereafter AdvT-1), climatologic mean temperature advection by anomalous wind (hereafter AdvT-2), and anomalous temperature advection by anomalous wind (hereafter AdvT-3), respectively. For the synoptic-scale analyses, if the grids with precipitation over 50 mm exceed 15% of the total grids over the YRB in one day, the day is selected as a YRB extreme precipitation event. Accordingly, 76 extreme precipitation events over the YRB were selected during the summer of 1979–2010 (based on the time span of the daily ERA dataset; due to the limited space, the list is not given) in our study. The synoptic-scale diagnoses were based on the composite results of all the YRB extreme precipitation events.

Figure 15 shows the diagnosed results based on Eq. (4) at the meridional–vertical section averaged over 106°–119°E. The second term (AdvT-2) on the right side of Eq. (4) was the largest contribution to the abnormal temperature advection in the YRB precipitation events in summer. This indicates that the mean states of the transport of warm air to the YRB in summer was a major source of maintaining the local ascending motion, which was responsible for the occurrence of the summer YRB precipitation extremes. An enhanced mean mei-yu front is closely associated with a larger seasonal mean temperature gradient $\nabla\overline{T}$ over the YRB (Fig. 16a), which can be beneficial to a stronger disturbed warm temperature advection $V'\nabla\overline{T}$ on the synoptic scale. A stronger disturbed $V'\nabla\overline{T}$ would be beneficial to a stronger ω' and more occurrences of the summer YRB precipitation extremes (Figs. 16b,c).

6. Summary and discussion

The mei-yu front is a unique phenomenon in East Asia. The associated quasi-stationary rainband is one of the key characteristics of the East Asian summer monsoon climate. In this study, we found that the frequency of summer precipitation extremes over the YRB was strongly associated with the mean state of the mei-yu front. Accompanied by excessive moisture transport to the YRB and an enhanced local ascending motion, a stronger mei-yu front suggested favorable conditions for local summer precipitation extremes.

As a typical dry–wet transitional region, the ICP exhibits a strong land–atmosphere coupling, in which the soil moisture anomaly has a large effect on the local thermal conditions. In spring, low levels of ICP soil moisture can suppress the surface evapotranspiration, increasing the local surface temperature. This soil moisture anomaly can be sustained through to the following summer due to its strong memory, and thus the anomalous surface heating will persist from spring to summer (Fig. 9; Gao et al. 2019). In general, this can lead to an uplifted local geopotential height in summer, potentially contributing to the westward shift of the WPSH (Fig. 10). On the other hand, high levels of ICP soil moisture will lead to a lower local temperature, and thus a decreased local geopotential height.

In the period before 1992, the summer geopotential height anomaly field at 500 hPa, which was related to the drier surface in spring over the ICP, extended zonally from the western Pacific Ocean to the ICP. Accordingly, the WPSH extended westward substantially. As a result, the southwesterly wind along the western rim of the abnormal WPSH was enhanced, bringing excessive warm and wet air across southern China to the YRB. This intensified the mei-yu front in summer, promoting the occurrence of intense precipitation. The risk of summer precipitation extremes over the YRB therefore increased with the abnormally drier ICP soil in spring, and vice versa.

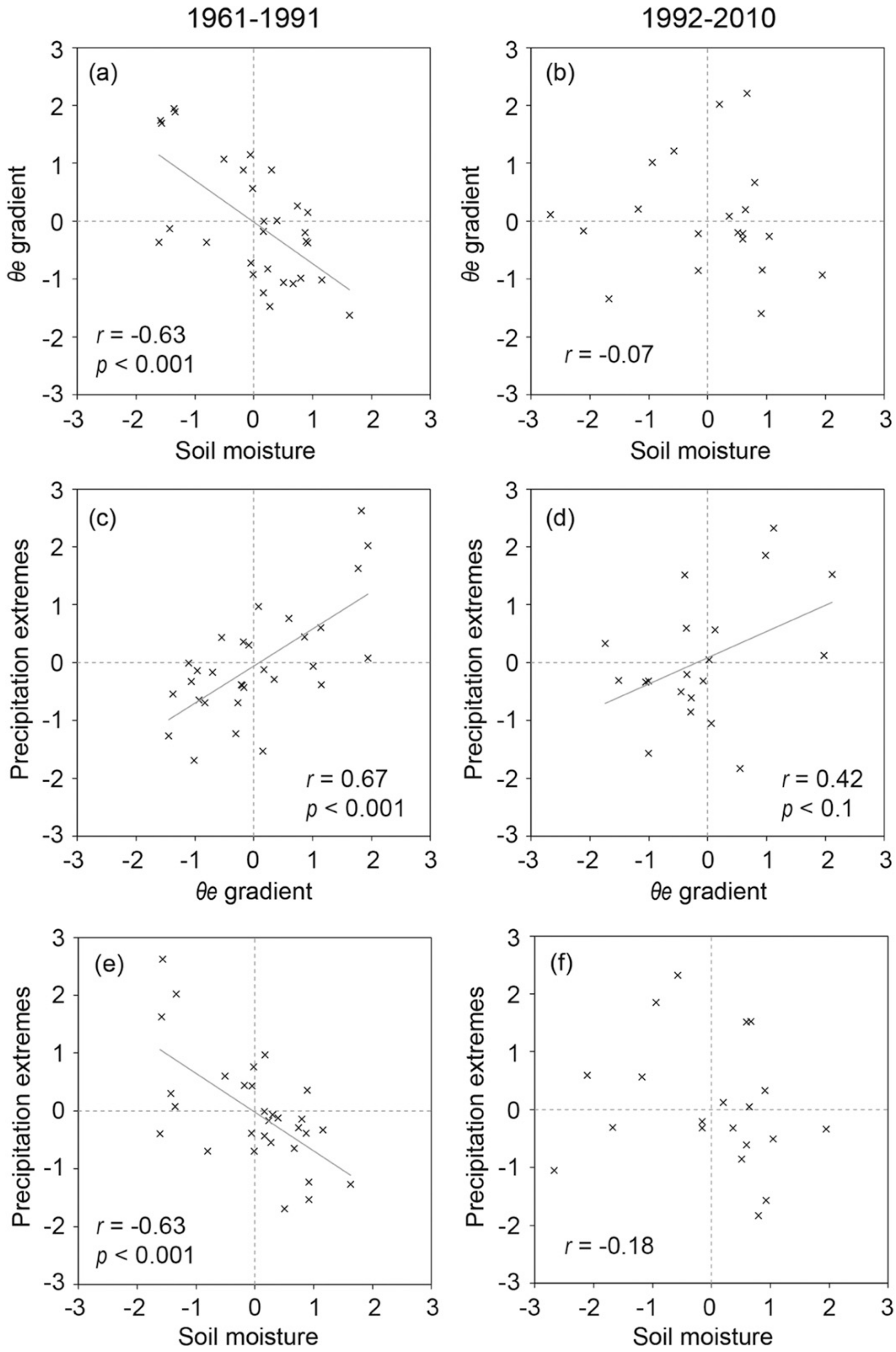

FIG. 14. Scatterplots (a) between the spring soil moisture averaged over the Indo-China Peninsula and summer $-d\theta_e/dy$ averaged over the Yangtze River basin, (c) between the summer $-d\theta_e/dy$ and precipitation extremes averaged over the YRB, and (e) between the spring soil moisture averaged over the ICP and summer precipitation extremes averaged over the YRB for the period of 1961–91. (b),(d),(f) As in (a), (c), and (e), respectively, but for the period of 1992–2010. The term r denotes the corresponding correlation coefficient for each panel. All data were linearly detrended and standardized for the correlation analysis.

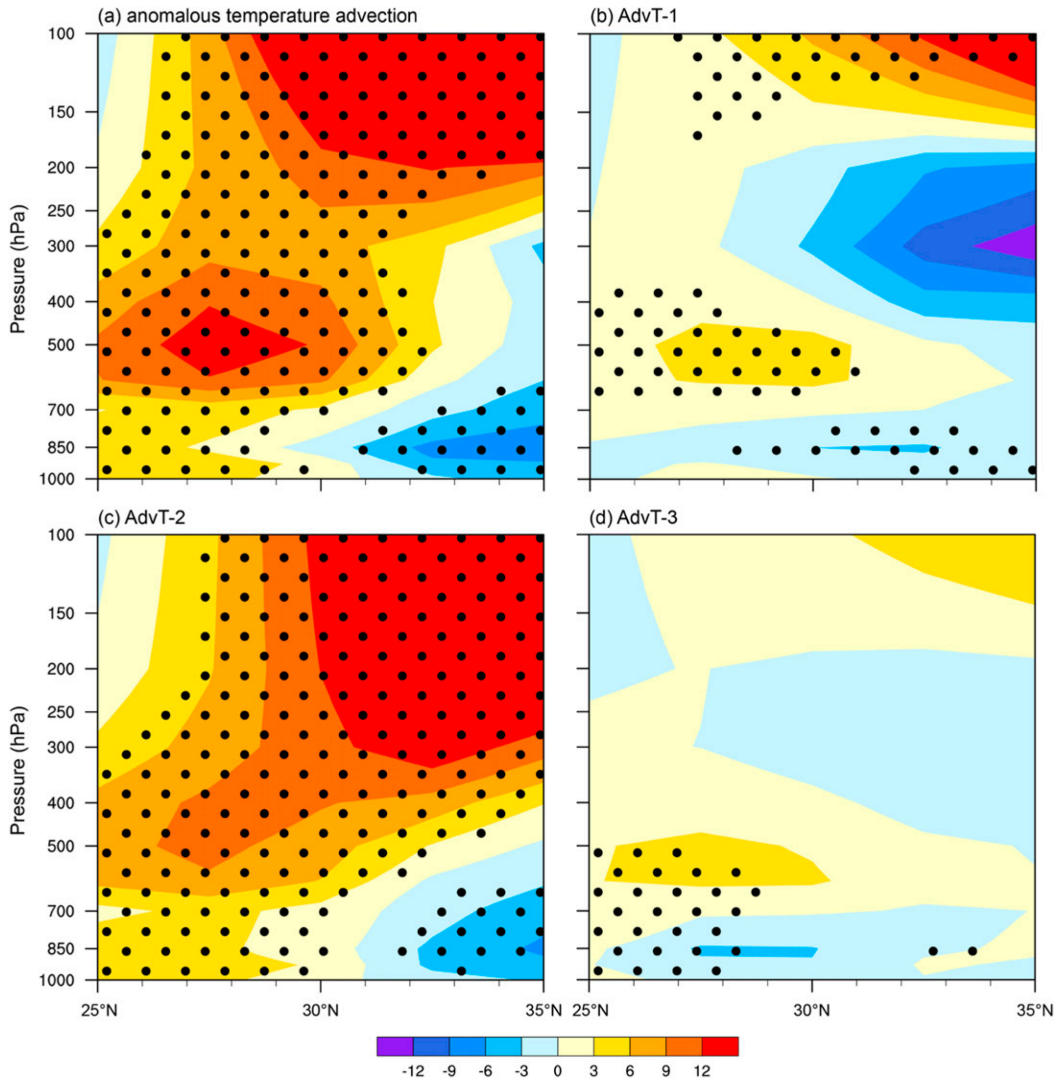

FIG. 15. Composites of (a) anomalous temperature advection [left term of Eq. (4)], (b) term AdvT-1, (c) term AdvT-2, and (d) term AdvT-3 averaged over 106°–119°E in the YRB extreme precipitation events during the summer of 1979–2010 (1×10^{-5} K s^{-1}). The dotted areas were significant with $p < 0.1$.

Since the early 1990s, although the anomalous heating induced by the identical ICP soil moisture anomaly was similar to the previous period, the response of the summer 500-hPa geopotential height anomaly displayed a different pattern. It was weaker and was located from the east of the Philippines to southern China. Compared with the climatic WPSH for the period of 1992–2010, the anomalous WPSH also extended westward, but had a much stronger body in the south. The East Asian summer monsoon was very sensitive to the strength and shape of the WPSH. The response of the southwesterly wind over southern China to the ICP soil moisture anomaly was also weakened, resulting in fewer changes in water vapor transported to the YRB. Consequently, there was basically no change in the mei-yu front associated with the spring ICP soil moisture anomaly. Hence, the influence of the spring ICP soil moisture on summer YRB precipitation extremes has weakened since the early 1990s.

Why did the similar abnormal surface heating induced by the ICP soil moisture anomaly lead to different responses of the large-scale monsoonal circulation and YRB precipitation extremes in the two subperiods? The East Asian summer monsoon system experienced an interdecadal change around the early 1990s under the background of climate change (Ding et al. 2008, 2009). The global temperature has increased dramatically in the last five decades (Dai 2011). The air temperature increased significantly over the tropical area during 1992–2010 compared to the earlier period (Fig. 17a), especially over the ICP land area. Accordingly, the climatic WPSH was stronger and extended westward during 1992–2010 (Fig. 17b), hampering

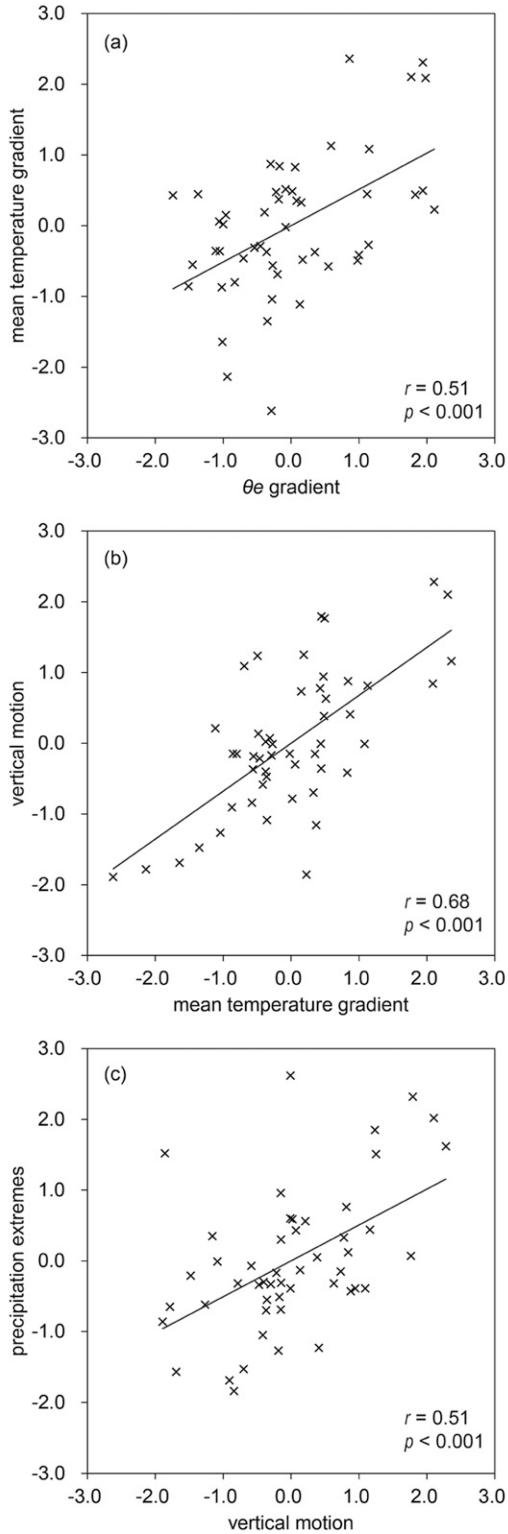

FIG. 16. Scatterplots (a) between the 700-hPa θ_e gradient $-d\theta_e/dy$ and mean temperature gradient $-\nabla\overline{T}$, (b) between the 700-hPa mean temperature gradient $-\nabla\overline{T}$ and disturbed vertical motion ω', and (c) between the disturbed vertical motion ω' and the occurrences of precipitation extremes in summer over the YRB for the period of 1961–2010. The term r denotes the corresponding correlation coefficient for each panel. All data were linearly detrended and standardized.

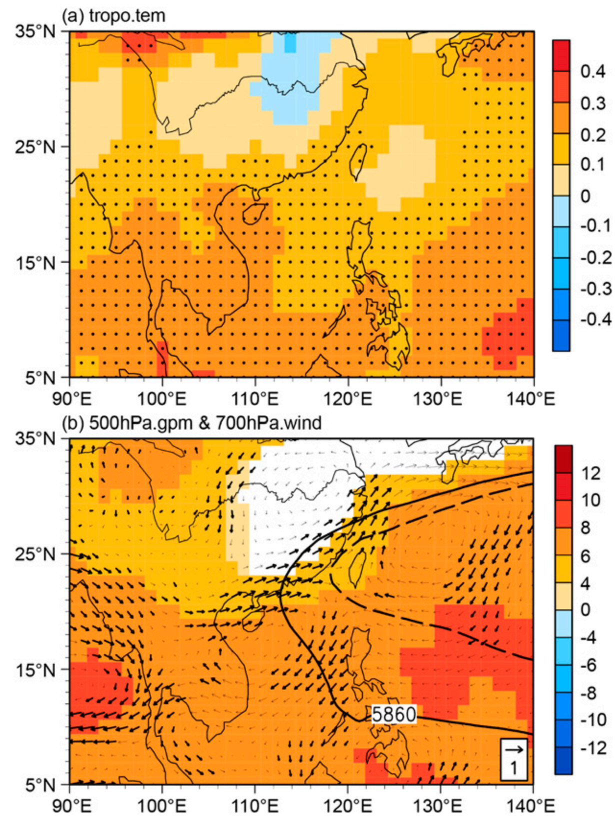

FIG. 17. (a) Interdecadal change (climatic mean of 1992–2010 minus that of 1961–91) of summer tropospheric temperature (averaged from 1000–300 hPa; colors; K). The dotted areas are significant at $p < 0.1$. (b) As in (a), but for the 500-hPa geopotential height (colors; gpm) and the 700 hPa wind (arrows; m s^{-1}). Only the areas of geopotential height and wind differences exceeding the significance level of $p < 0.1$ were shown with colors and bold arrows, respectively. The dashed and solid lines denote the climatic means of the 5860-gpm contour during 1961–91 and 1992–2010.

the northward advance of the East Asian summer monsoon. In this case, a similar surface heating over the ICP (Fig. 9) resulted in different responses of the monsoonal circulation (Fig. 12) and summer precipitation extremes over the YRB (Fig. 7). This was similar to previous results from both statistical analyses and model experiments, which showed that identical atmospheric heating over the tropical western Pacific could result in different responses of the monsoonal circulation/precipitation under different climatic mean states of the East Asian summer monsoon (Kosaka and Nakamura 2010; Li and Lu 2018).

Generally, the local precipitation is the primary driving factor of soil moisture anomaly, and is also closely linked to precipitation extremes. To check the robustness of our results, we calculated the spring precipitation and summer precipitation averaged over the ICP and YRB, respectively, by using the CRU dataset covering the period of 1961–2018. The correlation coefficient for the whole period was -0.26 ($p < 0.05$), which confirms that our results were still robust even including the recent eight years. Moreover, this correlation also exhibited an interdecadal change: it was strong during 1961–91 ($r = -0.51$, $p < 0.01$), while it almost vanished during 1992–2018 ($r = -0.03$).

The seasonal prediction of climate extremes over East Asia has always been difficult. Our study revealed the remote effect of the spring ICP soil moisture on the East Asian summer monsoon system, suggesting that it could be an important seasonal predictor of summer YRB precipitation extremes. This would benefit numerous people living in the YRB. However, the study also revealed that the effect has been experiencing an interdecadal weakening since the early 1990s, accompanied by a climatic shift of the East Asian summer monsoon system. The spring ICP soil moisture as a seasonal predictor should therefore be used with caution under climate change. Soil moisture anomalies are closely associated with local precipitation variations, which may be closely related to abnormal atmospheric circulations induced by SST anomalies. This could be thoroughly explored in the future.

Acknowledgments. This work was supported by the Fundamental Research Funds for the Central Universities (2018B03114 and 2019B18814), the Natural Science Foundation of China (41831175, 41905054, and 41861144013), the China Postdoctoral Science Foundation (2020T130168 and 2019M651665), and the Joint Open Project of Key Laboratory of Meteorological Disaster, Ministry of Education/Collaborative Innovation Center on Forecast and Evaluation of Meteorological Disasters, Nanjing University of Information Science and Technology (KLME202006).

REFERENCES

Cen, S., Y. Gong, X. Lai, and L. Peng, 2015: The relationship between the atmospheric heating source/sink anomalies of Asian monsoon and flood/drought in the Yangtze River basin in the Meiyu period. *J. Trop. Meteor.*, **21**, 352–360.

Chen, J., and L. Chen, 1991: Influence of ocean–continent distribution in the south part of Asia on the formation of Asian summer monsoon (in Chinese). *Quart. J. Appl. Meteor.*, **2**, 355–361.

Chen, Y., and P. Zhai, 2013: Persistent extreme precipitation events in China during 1951–2010. *Climate Res.*, **57**, 143–155, https://doi.org/10.3354/cr01171.

——, and ——, 2015: Synoptic-scale precursors of the East Asia/Pacific teleconnection pattern responsible for persistent extreme precipitation in the Yangtze River Valley. *Quart. J. Roy. Meteor. Soc.*, **141**, 1389–1403, https://doi.org/10.1002/qj.2448.

——, and ——, 2016: Mechanisms for concurrent low-latitude circulation anomalies responsible for persistent extreme precipitation in the Yangtze River Valley. *Climate Dyn.*, **47**, 989–1006, https://doi.org/10.1007/s00382-015-2885-6.

Cheng, S. J., X. D. Guan, J. P. Huang, F. Ji, and R. X. Guo, 2015: Long-term trend and variability of soil moisture over East Asia. *J. Geophys. Res. Atmos.*, **120**, 8658–8670, https://doi.org/10.1002/2015jd023206.

Dai, A., 2011: Drought under global warming: A review. *Wiley Interdiscip. Rev.: Climate Change*, **2**, 45–65, https://doi.org/10.1002/wcc.81.

Ding, Y., J. Liu, Y. Sun, Y. Liu, J. He, and Y. Song, 2007: A study of the synoptic-climatology of the Meiyu system in East Asia (in Chinese). *Chin. J. Atmos. Sci.*, **31**, 1082–1101.

——, Z. Wang, and Y. Sun, 2008: Inter-decadal variation of the summer precipitation in East China and its association with decreasing Asian summer monsoon. Part I: Observed evidences. *Int. J. Climatol.*, **28**, 1139–1161, https://doi.org/10.1002/joc.1615.

——, Y. Sun, Z. Wang, Y. Zhu, and Y. Song, 2009: Inter-decadal variation of the summer precipitation in China and its association with decreasing Asian summer monsoon. Part II: Possible causes. *Int. J. Climatol.*, **29**, 1926–1944, https://doi.org/10.1002/joc.1759.

Dirmeyer, P. A., 2011: The terrestrial segment of soil moisture–climate coupling. *Geophys. Res. Lett.*, **38**, L16702, https://doi.org/10.1029/2011GL048268.

Douville, H., 2002: Influence of soil moisture on the Asian and African monsoons. Part II: Interannual variability. *J. Climate*, **15**, 701–720, https://doi.org/10.1175/1520-0442(2002)015<0701:IOSMOT>2.0.CO;2.

——, F. Chauvin, and H. Broqua, 2001: Influence of soil moisture on the Asian and African monsoons. Part I: Mean monsoon and daily precipitation. *J. Climate*, **14**, 2381–2403, https://doi.org/10.1175/1520-0442(2001)014<2381:IOSMOT>2.0.CO;2.

Ek, M. B., K. E. Mitchell, Y. Lin, E. Rogers, P. Grunmann, V. Koren, G. Gayno, and J. D. Tarpley, 2003: Implementation of Noah land surface model advances in the National Centers for Environmental Prediction operational mesoscale Eta model. *J. Geophys. Res.*, **108**, 8851, https://doi.org/10.1029/2002JD003296.

Feng, L., T. Li, and W. Yu, 2014: Cause of severe droughts in Southwest China during 1951–2010. *Climate Dyn.*, **43**, 2033–2042, https://doi.org/10.1007/s00382-013-2026-z.

Fischer, E. M., S. I. Seneviratne, P. L. Vidale, D. Lüthi, and C. Schär, 2007: Soil moisture–atmosphere interactions during the 2003 European summer heat wave. *J. Climate*, **20**, 5081–5099, https://doi.org/10.1175/JCLI4288.1.

Gao, C., and Coauthors, 2019: Land–atmosphere interaction over the Indo-China Peninsula during spring and its effect on the following summer climate over the Yangtze River basin. *Climate Dyn.*, **53**, 6181–6198, https://doi.org/10.1007/s00382-019-04922-x.

Gao, H., W. Jiang, and W. Li, 2015: Changed relationships between the East Asian summer monsoon circulations and the summer rainfall in eastern China. *J. Meteor. Res.*, **28**, 1075–1084, https://doi.org/10.1007/s13351-014-4327-5.

He, J., J. Ju, Z. Wen, J. Lü, and Q. Jin, 2007: A review of recent advances in research on Asian monsoon in China. *Adv. Atmos. Sci.*, **24**, 972–992, https://doi.org/10.1007/s00376-007-0972-2.

Holton, J. R., 2004: *An Introduction to Dynamic Meteorology*. 4th ed. Elsevier Academic Press, 535 pp.

Huang, R., Y. Xu, P. Wang, and L. Zhou, 1998: The features of the catastrophic flood over the Changjiang River basin during the summer of 1998 and cause exploration (in Chinese). *Climatic Environ. Res.*, **3**, 300–313.

Jin, Q., J. He, L. Chen, and C. Zhu, 2006: Impact of ocean–continent distribution over Southern Asia on the formation of summer monsoon. *Acta Meteor. Sin.*, **20**, 95–108.

Kobayashi, S., and Coauthors, 2015: The JRA-55 reanalysis: General specifications and basic characteristics. *J. Meteor. Soc. Japan*, **93**, 5–48, https://doi.org/10.2151/jmsj.2015-001.

Kosaka, Y., and H. Nakamura, 2010: Mechanisms of meridional teleconnection observed between a summer monsoon system and a subtropical anticyclone. Part I: The Pacific–Japan pattern. *J. Climate*, **23**, 5085–5108, https://doi.org/10.1175/2010JCLI3413.1.

Li, W., L. Duan, Y. Luo, T. Liu, and B. Scharaw, 2018: Spatiotemporal characteristics of extreme precipitation regimes in the eastern inland river basin of Inner Mongolian plateau, China. *Water*, **10**, 35, https://doi.org/10.3390/w10010035.

Li, X., and R. Lu, 2017: Extratropical factors affecting the variability in summer precipitation over the Yangtze River basin, China. *J. Climate*, **30**, 8357–8374, https://doi.org/10.1175/JCLI-D-16-0282.1.

——, and ——, 2018: Subseasonal change in the seesaw pattern of precipitation between the Yangtze River basin and the tropical western North Pacific during summer. *Adv. Atmos. Sci*, **35**, 1231–1242, https://doi.org/10.1007/s00376-018-7304-6.

Liu, L., R. Zhang, and Z. Zuo, 2017: Effect of spring precipitation on summer precipitation in eastern China: Role of soil moisture. *J. Climate*, **30**, 9183–9194, https://doi.org/10.1175/JCLI-D-17-0028.1.

Lu, R., 2004: Associations among the components of the East Asian summer monsoon system in the meridional direction. *J. Meteor. Soc. Japan*, **82**, 155–165, https://doi.org/10.2151/jmsj.82.155.

Ma, J., S. Yang, and Z. Wang, 2018: Influence of spring soil moisture anomaly in the Indo-China peninsula on the establishment and development of Asian tropical summer monsoon (in Chinese). *Meteor. Environ. Sci.*, **41**, 19–30.

Ninomiya, K., and Y. Shibagaki, 2007: Multi-scale features of the Meiyu-baiu front and associated precipitation systems. *J. Meteor. Soc. Japan*, **85B**, 103–122, https://doi.org/10.2151/jmsj.85B.103.

Piao, S., L. Yin, X. Wang, P. Ciais, S. Peng, Z. Shen, and S. I. Seneviratne, 2009: Summer soil moisture regulated by precipitation frequency in China. *Environ. Res. Lett.*, **4**, 044012, https://doi.org/10.1088/1748-9326/4/4/044012.

Rayner, N., D. E. Parker, E. Horton, C. K. Folland, L. V. Alexander, D. Rowell, E. Kent, and A. Kaplan, 2003: Global analyses of sea surface temperature, sea ice, and night marine air temperature since the late nineteenth century. *J. Geophys. Res.*, **108**, 4407, https://doi.org/10.1029/2002JD002670.

Ren, Z., M. Zhang, S. Wang, F. Qiang, X. Zhu, and L. Dong, 2014: Changes in daily extreme precipitation events in South China from 1961 to 2011. *J. Geogr. Sci.*, **25**, 58–68, https://doi.org/10.1007/s11442-015-1153-3.

Rodell, M., and Coauthors, 2004: The Global Land Data Assimilation System. *Bull. Amer. Meteor. Soc.*, **85**, 381–394, https://doi.org/10.1175/BAMS-85-3-381.

Roeckner, E., and Coauthors, 1996: The atmospheric general circulation model, ECHAM-4: Model description and simulation of present-day climate. Max-Planck-Institut für Meteorologie Rep. 218, 90 pp.

Sampe, T., and S.-P. Xie, 2010: Large-scale dynamics of the meiyu-baiu rainband: Environmental forcing by the westerly jet. *J. Climate*, **23**, 113–134, https://doi.org/10.1175/2009JCLI3128.1.

Sheffield, J., G. Goteti, and E. F. Wood, 2006: Development of a 50-year high-resolution global dataset of meteorological forcings for land surface modeling. *J. Climate*, **19**, 3088–3111, https://doi.org/10.1175/JCLI3790.1.

Tao, W., G. Huang, K. Hu, H. Gong, G. Wen, and L. Liu, 2016: A study of biases in simulation of the Indian Ocean basin mode and its capacitor effect in CMIP3/CMIP5 models. *Climate Dyn.*, **46**, 205–226, https://doi.org/10.1007/s00382-015-2579-0.

Wang, B., and LinHo, 2002: Rainy season of the Asian-Pacific summer monsoon. *J. Climate*, **15**, 386–398, https://doi.org/10.1175/1520-0442(2002)015<0386:RSOTAP>2.0.CO;2.

——, R. Wu, and X. Fu, 2000: Pacific–East Asian teleconnection: How does ENSO affect East Asian climate? *J. Climate*, **13**, 1517–1536, https://doi.org/10.1175/1520-0442(2000)013<1517:PEATHD>2.0.CO;2.

Wang, H., and H. Chen, 2012: Climate control for southeastern China moisture and precipitation: Indian or East Asian monsoon? *J. Geophys. Res.*, **117**, D12109, https://doi.org/10.1029/2012JD017734.

Wang, L., and L. Chen, 2017: Interannual variation of the Asian-Pacific oscillation. *Dyn. Atmos. Oceans*, **77**, 17–25, https://doi.org/10.1016/j.dynatmoce.2016.10.009.

——, and T. Li, 2020: Effect of vertical moist static energy advection on MJO eastward propagation: Sensitivity to analysis domain. *Climate Dyn.*, **54**, 2029–2039, https://doi.org/10.1007/s00382-019-05101-8.

——, ——, E. Maloney, and B. Wang, 2017: Fundamental causes of propagating and non-propagating MJOs in MJOTF/GASS models. *J. Climate*, **30**, 3743–3769, https://doi.org/10.1175/JCLI-D-16-0765.1.

——, ——, and N. Tomoe, 2018: Impact of Rossby and Kelvin wave components on MJO eastward propagation. *J. Climate*, **31**, 6913–6931, https://doi.org/10.1175/JCLI-D-17-0749.1.

Webster, P. J., 1983: Mechanisms of monsoon low-frequency variability: Surface hydrological effects. *J. Atmos. Sci.*, **40**, 2110–2124, https://doi.org/10.1175/1520-0469(1983)040<2110:MOMLFV>2.0.CO;2.

Wen, N., Z. Liu, and L. Li, 2018: Direct ENSO impact on East Asian summer precipitation in the developing summer. *Climate Dyn.*, **52**, 6799–6815, https://doi.org/10.1007/s00382-018-4545-0.

Wen, Z., L. Dong, L. Wu, and W. Chen, 2007: The characteristics of 30–60 day oscillation and its relation to the durative rainstorm in Guangdong (in Chinese). *Acta Sci. Nat. Univ. Sunyatseni*, **46**, 98–103.

Wu, B., R. Zhang, B. Wang, and R. D'Arrigo, 2009: On the association between spring Arctic sea ice concentration and Chinese summer rainfall. *Geophys. Res. Lett.*, **36**, L09501, https://doi.org/10.1029/2009GL037299.

Wu, G., and Coauthors, 2007: The influence of mechanical and thermal forcing by the Tibetan Plateau on Asian climate. *J. Hydrometeor.*, **8**, 770–789, https://doi.org/10.1175/JHM609.1.

Wu, L., and J. Zhang, 2013: Asymmetric effects of soil moisture on mean daily maximum and minimum temperatures over eastern China. *Meteor. Atmos. Phys.*, **122**, 199–213, https://doi.org/10.1007/s00703-013-0284-2.

Wu, T.-W., and Z.-A. Qian, 2003: The relation between the Tibetan winter snow and the Asian summer monsoon and rainfall: An observational investigation. *J. Climate*, **16**, 2038–2051, https://doi.org/10.1175/1520-0442(2003)016<2038:TRBTTW>2.0.CO;2.

Xiang, B., B. Wang, A. Lauer, J. Y. Lee, and Q. Ding, 2014: Upper tropospheric warming intensifies sea surface warming. *Climate Dyn.*, **43**, 259–270, https://doi.org/10.1007/s00382-013-1928-0.

Xie, S.-P., K. Hu, J. Hafner, H. Tokinaga, Y. Du, G. Huang, and T. Sampe, 2009: Indian Ocean capacitor effect on Indo–western Pacific climate during the summer following El Niño. *J. Climate*, **22**, 730–747, https://doi.org/10.1175/2008JCLI2544.1.

——, Y. Kosaka, Y. Du, K. Hu, J. S. Chowdary, and G. Huang, 2016: Indo-western Pacific Ocean capacitor and coherent climate anomalies in post-ENSO summer: A review. *Adv. Atmos. Sci.*, **33**, 411–432, https://doi.org/10.1007/s00376-015-5192-6.

Yang, K., J. Zhang, L. Wu, and J. Wei, 2019: Prediction of summer hot extremes over the middle and lower reaches of the Yangtze River valley. *Climate Dyn.*, **52**, 2943–2957, https://doi.org/10.1007/s00382-018-4302-4.

Zhai, P., X. Zhang, W. Hui, and X. Pan, 2005: Trends in total precipitation and frequency of daily precipitation extremes over China. *J. Climate*, **18**, 1096–1108, https://doi.org/10.1175/JCLI-3318.1.

Zhang, R., and Z. Zuo, 2011: Impact of spring soil moisture on surface energy balance and summer monsoon circulation over East Asia and precipitation in East China. *J. Climate*, **24**, 3309–3322, https://doi.org/10.1175/2011JCLI4084.1.

——, R. Zhang, and Z. Zuo, 2017: Impact of Eurasian spring snow decrement on East Asian summer precipitation. *J. Climate*, **30**, 3421–3437, https://doi.org/10.1175/JCLI-D-16-0214.1.

Zhang, W. J., and Coauthors, 2016: Unraveling El Niño's impact on the East Asian monsoon and Yangtze River summer flooding. *Geophys. Res. Lett.*, **43**, 11 375–11 382, https://doi.org/10.1002/2016GL071190.

Zhang, Y., and Y. Qian, 2002: Mechanism of thermal features over the Indo-China Peninsula and possible effects on the onset of the South China Sea monsoon. *Adv. Atmos. Sci.*, **19**, 885–900, https://doi.org/10.1007/s00376-002-0053-5.

Zhou, Y., G. Deng, H. Chen, and Z. Chen, 2005: Synoptic features of the second Meiyu period in 1998 over China. *J. Meteor. Res.*, **19**, 31–43.

Zuo, Z., and R. Zhang, 2016: Influence of soil moisture in eastern China on the East Asian summer monsoon. *Adv. Atmos. Sci.*, **33**, 151–163, https://doi.org/10.1007/s00376-015-5024-8.